

Optical deflection of molecules

Hirofumi Sakai,^{1,2} A. Tarasevitch,^{1,3} J. Danilov,^{1,3} H. Stapelfeldt,^{1,*} R. W. Yip,^{1,4} C. Ellert,¹ E. Constant,^{1,5} and P. B. Corkum¹

¹*Steacie Institute for Molecular Sciences, National Research Council of Canada, Ottawa, Ontario, Canada K1A 0R6*

²*Electrotechnical Laboratory, 1-1-4 Umezono, Tsukuba, Ibaraki 305, Japan*

³*International Laser Centre, Moscow State University, Moscow, Russia*

⁴*Département de Chimie, Université du Québec à Montréal, Montreal, Québec, Canada H3C 3P8*

⁵*Département de Physique, Faculté des Sciences, Université de Sherbrooke, Sherbrooke, Québec, Canada J1K 2R1*

(Received 18 August 1997)

When intense light interacts with a molecule it induces a force proportional to the gradient of the Stark shift. We use this nonresonant force to deflect I_2 and CS_2 molecules. We trace the direction of molecules in a molecular beam, showing that the molecules that pass near the center of a 1.06- μm or 10.6- μm laser beam will focus. We predict that Stark shifts on the order of 50 meV can be obtained for all small molecules and atoms while maintaining ionization rates below 10^6 s^{-1} . Among the devices that can be based on the nonresonant Stark shift are molecular accelerators and molecular quantum wires. [S1050-2947(98)01503-0]

PACS number(s): 42.50.Vk, 33.80.Ps, 51.70.+f

I. INTRODUCTION

Intense laser fields apply forces to molecules that are strong enough to control both the internal and external molecular variables [1–5]. Experimentally, we study the control over the trajectory of a molecule using the force resulting from the gradient of the nonresonant laser-induced Stark shift. This force arises from the gradient of the interaction of the laser-induced dipole moment with the laser field. The potential well depths that we measure are approximately 10 meV deep and we predict potential well depths of 50 meV or more for molecules and atoms at intensities where the ionization rate is less than 10^6 s^{-1} . Theoretically, we discuss characteristics of the new class of molecular devices that can be based on the nonresonant dipole force.

We demonstrate laser-induced forces with both 1.06 μm (YAG) [6] and 10.6 μm (CO_2) light interacting with carbon disulfide (CS_2) and iodine (I_2) molecules and show that these light beams can be used as molecular lenses. By choosing two wavelengths and two molecules we emphasize the generality of the nonresonant dipole force. On one hand, we have chosen 1.06 μm to direct our thoughts towards future experiments where very small focal spots ($\approx 0.5 \mu\text{m}$) are achieved. As we will discuss in the concluding section, such small focal spots will allow us to control the position of molecules with almost atomic scale precision. For example, we show that such exotic new devices as molecular quantum wires can be constructed. On the other hand, we have chosen 10.6- μm light since the interaction of intense infrared light with small molecules and atoms is especially simple [2,7]. For example, we know that midinfrared light should be the least intrusive strong field source [2] for manipulating a small molecule. With infrared light, ionization, excitation, and dissociation will all be minimized since resonances are unlikely to play a significant role in the multiphoton ioniza-

tion of the molecule and it is well known that small neutral molecules cannot be efficiently vibrationally excited by mid-infrared light [8]. Consequently, the maximum fields that we calculate by approximating multiphoton ionization by tunneling is appropriate for 10- μm light and may slightly overestimate the appropriate fields at 1.06 μm .

Our experimental approach gives us the opportunity to study the deflection of molecules with precision. We trace the deviation of the molecular trajectories caused by their interaction with either the CO_2 or YAG laser field at different offsets from the center of the molecular lens. Thus, the information that we get is analogous to the information obtained in optical ray tracing.

This work should be considered in the context of the large international effort in manipulation and control of the position and velocity of electrons [9], atoms [10], and nano or microscopic particles (optical tweezers) [11,12]. We will show that molecular optics can be developed in direct analogy with atomic optics and our experimental approach to molecular diagnostics based on multiphoton ionization introduces a general method for performing molecular optics experiments.

II. OVERVIEW OF THE EXPERIMENT

A schematic of the experimental layout is shown in Fig. 1. Iodine or carbon disulfide molecules from a pulsed molecular beam are injected into a vacuum chamber along a direction perpendicular to the flight axis of a time-of-flight mass spectrometer. An intense YAG or CO_2 beam, traveling perpendicular to both the molecular beam and time-of-flight axis, interacts with the molecular beam. Those molecules that pass through the deflecting beam experience the laser-induced dipole force.

We label those molecules to be measured by placing the deflecting laser beam just upstream of the focus of a femtosecond diagnostic laser beam. The femtosecond pulse ionizes the molecules producing singly charged molecular ions by nonresonant multiphoton ionization. Due to the highly non-

*Present address: Department of Chemistry, Aarhus University, Langelandsgade 140, DK-8000 Aarhus C, Denmark.

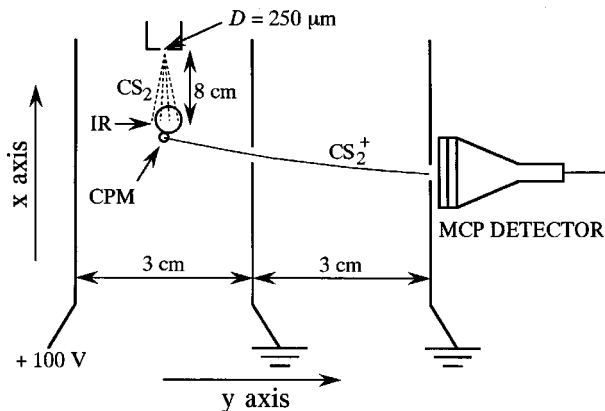


FIG. 1. Schematic of the experimental arrangement of the target chamber viewed in the direction of the laser beam (z axis).

linear nature of multiphoton ionization the measurement is confined to the high intensity region [13] of the femtosecond beam. The femtosecond beam is focused to a smaller spot than the deflection beam. With our experimental procedure we have more than 10 resolution elements across the central portion of the focus of the CO_2 laser.

Only molecules that come from the small nozzle (diameter $250 \mu\text{m}$) and pass through the small focus of the probe laser 8 cm below the nozzle can be ionized by the colliding-pulse mode-locked (CPM) pulse. This ensures that the molecules that are studied initially have a very small velocity in the direction of the time-of-flight axis. Molecules that gain more energy from the deflection beam than the initial transverse energy spread are observable through a difference in arrival times of the singly charged molecular ions compared to the arrival time without the deflection beam. By scanning the diagnostic beam with respect to the center of the deflecting beam focus, the molecular deflection is measured as a function of the position inside the deflecting beam. Our measurement is the molecular analog of ray tracing in optics and we show the molecular beam will focus.

III. EXPERIMENTAL CONSIDERATIONS

A 10-Hz pulsed beam of I_2 or CS_2 molecules was used directly or was seeded in an argon or neon jet expanding from the initial pressure of 1 atm into the vacuum chamber with the average operating pressure of about 10^{-6} Torr. For I_2 , a container filled with solid I_2 at room temperature was placed directly before the pulsed nozzle (vapor pressure of I_2 at room temperature is about 0.3 Torr) while for CS_2 a partial gas pressure of 25 Torr was used. The nozzle diameter of the jet was $250 \mu\text{m}$.

The molecules entered a time-of-flight mass spectrometer with the molecular beam axis (the x axis) perpendicular to the flight axis (the y axis). The molecular velocity is given by [14]

$$v_x \approx \left(\frac{2k}{M} \frac{\gamma}{\gamma-1} T_0 \right)^{1/2}, \quad (1)$$

where k is the Boltzmann constant, M is the mass of the buffer gas atoms, γ is the specific heat ratio of the buffer gas,

and T_0 is the initial temperature. For Ar at $T_0 = 300$ K, Eq. (1) predicts $v_x = 560$ m/s and for neon it predicts 790 m/s. For iodine molecules buffered with neon, we measured $v_x = 800$ m/s, in excellent agreement with the prediction.

Either a Nd:YAG or a CO_2 laser beam (described in Secs. IV and VI, respectively) intersected the molecular beam approximately 8 cm below the nozzle, exerting a dipole force on those molecules that pass through the focus. The dipole force accelerated the molecules perpendicular to the initial direction. The velocity change was measured by ionizing the molecules and using a time-of-flight mass spectrometer to determine the velocity of the ions. The time-of-flight mass spectrometer consisted of an accelerating region (approximately 30 V/cm) defined by two plates separated by 3 cm and an equal length field-free drift region. After passage through the field-free region the ions were accelerated to 2 keV. Molecular ions with an initial transverse velocity component towards the detector arrived at the detector earlier than a zero transverse velocity ion. Similarly, ions with transverse velocity away from the detector arrived later.

The 80-fs duration ionizing pulse originating from a 10-Hz amplified CPM dye laser [15] contained $0.66 \mu\text{J}$ per pulse and was focused to a spot size of $\omega_0 \sim 2.5 \mu\text{m}$ corresponding to a peak intensity of $8 \times 10^{13} \text{ W/cm}^2$. We operated the laser with just high enough intensity to produce the singly charged molecular ion by nonresonant multiphoton ionization. It is possible to use multiphoton ionization to select and label the molecules of interest since ionization does not change the velocity of the molecule significantly [16]. Thus, measuring the ion velocity is equivalent to measuring the neutral molecule velocity. Using multiphoton ionization is important because the multiphoton ionization rate is a highly nonlinear function of the laser intensity so the measurement can be localized in both space and time.

The dye amplifier was pumped with $0.53 \mu\text{m}$ light from a frequency-doubled Nd:YAG laser. The undoubled radiation ($1.06 \mu\text{m}$) from the same YAG laser was used to deflect the molecules. We introduced a delay between the deflection and the CPM pulse to ensure that the femtosecond ionization occurred without the strong infrared pulse present. This delay required the focal spots of the two beams to be offset in the direction of the molecular beam. With this experimental arrangement, the CPM laser could probe the spatial dependence of the induced dipole force along direction of the time-of-flight axis simply by moving its focus with respect to the focal volume of the deflection beam. Although the mass spectrometer was designed so that the flight time was insensitive to the position where ionization occurred (space focusing), whenever we moved the relative position of the deflection and probe beams the probe beam was kept fixed so as to keep the measurement conditions constant.

IV. EXPERIMENTAL RESULTS WITH 1.06- μm DEFLECTION BEAM

The 10-Hz Nd:YAG laser ($\lambda = 1.064 \mu\text{m}$) produced 14-ns [full width at half maximum (FWHM)] pulses and we used these pulses in the energy range of 10 mJ. Figure 2 shows the experimental arrangement used with the YAG beam. The YAG (deflection) and dye (measurement) beams passed through two independent 1-m lenses and were combined with a dichroic beam splitter before reaching foci 1 m in front of the vacuum chamber. Here, the focal spot inten-

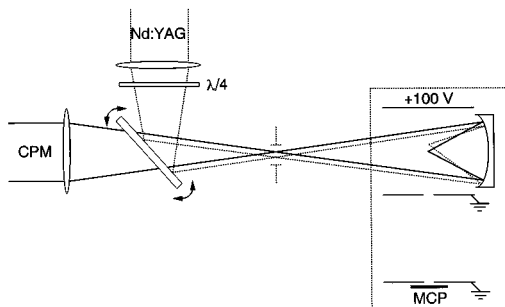


FIG. 2. Experimental schematic showing the optical arrangement used to position the YAG (deflection) beam and the dye (measurement) beam. The deflection and measurement beams are offset in both space and time.

sity distribution of the YAG was measured to be Gaussian and the beams were positioned with respect to each other. The foci in the target chamber were obtained with an $f/2$, on-axis, 5-cm focal-length parabolic mirror, which produced a 20 times reduced image of the measured focal spots. The YAG beam was focused in the center of the chamber to an $\omega_0 = 7 \mu\text{m}$ Gaussian focal spot giving a peak intensity, $I_0 \sim 9 \times 10^{11} \text{ W/cm}^2$ at 10 mJ. At this intensity the YAG pulse produced some CS_2 and I_2 ions. These ions arrive at the detector earlier than the ions produced by the femtosecond pulse since the YAG pulse arrives 25 ns before the femtosecond probe pulse. Thus, the peaks are clearly distinguished.

Since our velocity measurement is restricted to those molecules that pass through the very small focal spot of the CPM laser, in the absence of the deflection pulse, we expect the transverse velocity distribution of the molecular beam to be very narrow. The initial velocity spread along the time-of-flight axis, Δv_y^{init} , is determined by $\Delta v_y^{\text{init}} = D/(l/v_x)$ where $D = 250 \mu\text{m}$ is the diameter of the nozzle, $l = 8 \text{ cm}$ is the distance from the nozzle to the laser focus, and v_x is the longitudinal velocity of the CS_2 or I_2 molecules. The estimated velocity spread $\Delta v_y^{\text{init}} \cong 1.4 \text{ m/s}$ for unbuffered CS_2 is typical. It corresponds to a lateral kinetic energy of approximately $0.2 \mu\text{eV}$. In the experiment the FWHM of the peak is $\sim 3.4 \text{ ns}$, corresponding to a y -axis velocity $\Delta v_y^{\text{init}} = \pm 7.2 \text{ m/s}$ for CS_2 and $\Delta v_y^{\text{init}} = \pm 3 \text{ m/s}$ for I_2 . This value is the resolution limit of our time-of-flight spectrometer.

Time-of-flight spectra obtained with or without $1.06\text{-}\mu\text{m}$ light at a peak intensity of $1 \times 10^{12} \text{ W/cm}^2$ are shown in Fig. 3 for CS_2 molecules. Each spectrum is the average of 1000 shots. The solid curve shows the arrival time for the CS_2 molecules without the deflecting YAG laser. The dashed and dotted curves show the arrival times when the molecular beam crosses the deflection beam at approximately $\pm \omega_0/2$. The dashed (dotted) curve shows results obtained for molecules deflected towards (away from) the microchannel plate detector. As indicated in the figure, if the molecule is deflected away from the detector by the attractive central potential it should arrive later than if the molecule is deflected towards the detector. To ensure that the flight time is always the same without the deflection laser present, the focus of the CPM beam is not moved. Instead, we moved the focus of the deflecting laser beam.

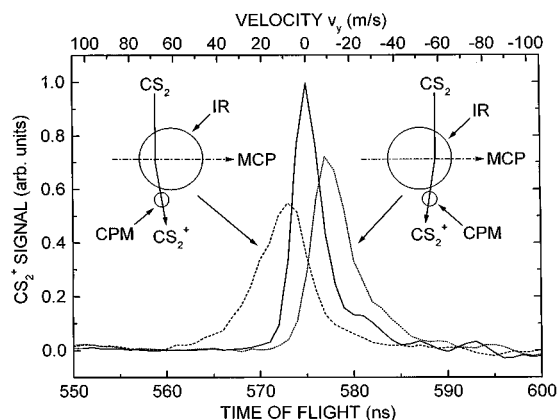


FIG. 3. Portion of the time of flight spectrum showing the time of arrival of the undeflected beam (solid curve) and the deflected beams (dashed and dotted curves). A schematic shows the relative placement of the focus of the deflecting laser and the measurement laser. Deviations of the arrival time of a zero transverse velocity molecule from the arrival time of a deflected molecule allow the transverse velocity to be measured. The horizontal scale shows both the arrival time and the velocity.

The shift of arrival times $\Delta\tau$ (with respect to the undeflected molecules) measured at the center position of the half maximum of the time-of-flight spectrum is plotted in Fig. 4 as a function of the position of the deflection beam. The results for the deflection of I_2 (expanded in the jet using an argon buffer gas) are shown in Fig. 4(a) and for CS_2 (expanded in a neon buffer gas) in Fig. 4(b). In both cases the laser intensity was approximately 10^{12} W/cm^2 . The vertical axes show the change in the arrival time and the corresponding transverse velocity $\Delta v_y = \Delta\tau eV/mL$, acquired in the deflecting field. The charge and mass of the molecular ion are denoted by e and m , V is the extracting voltage, and $L = 3 \text{ cm}$ is the separation between the first two plates of the time-of-flight spectrometer. For the measurements in Fig. 3 the V/L was 33 V/cm .

Figure 4(a) shows data, plotted with open and solid circles, obtained on two successive runs indicating the accuracy of the iodine data. Figure 4(b) contains plots obtained for linear and circular polarization. Experimentally, the $\lambda/4$ wave plate in the $1.06\text{-}\mu\text{m}$ beam path is rotated without changing the light intensity. The good agreement between the deflection measured with both polarization shows that the molecules do not align.

The experimental results allow us to determine the depth of the potential well produced by the intense laser beam. When a molecule enters the YAG laser focus a dipole moment is induced. The interaction of this dipole and the field results in a Stark shift U of the ground state of the molecule given by [17]

$$U(x, y, z, t) = -\frac{1}{4} \alpha E^2(x, y, z, t), \quad (2)$$

where $E(x, y, z, t)$ is the space- and time-dependent pulse envelope of the deflecting laser field. Equation (2) includes a time average over one period of the laser field and neglects any effect of alignment of the molecule by averaging over all

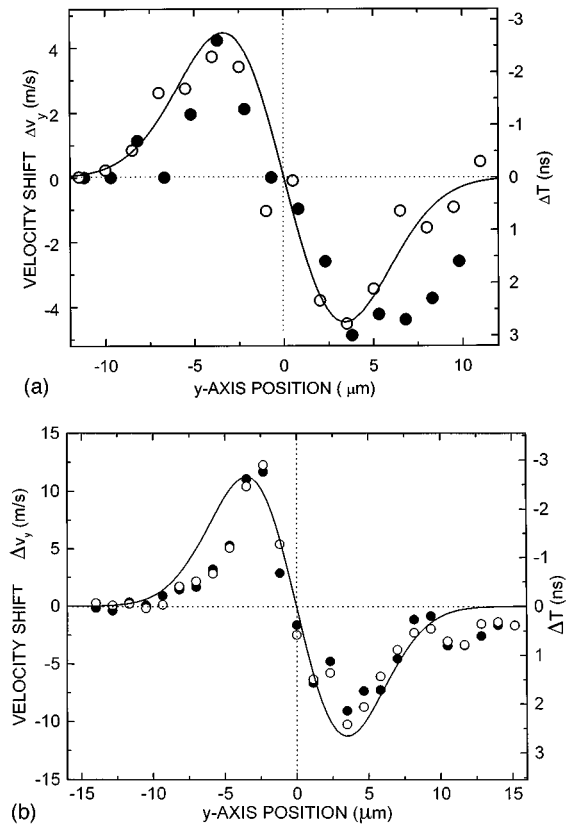


FIG. 4. Change in flight time caused by deflection of the molecular beam by the deflection beam and the associated change in transverse velocity of the molecular beam plotted as a function of the relative position of the focus of the deflecting and the ionizing laser beams. The derivative of the measured focal distribution is also shown by the solid curve. (a) Data obtained for I_2 with linear polarized light. The open and filled circles correspond to two successive scans with realignment. (b) Data for CS_2 with the deflection laser polarized linearly, or circularly (\bullet). In both cases the expansion of the CS_2 molecules was buffered with neon.

angles [$\alpha = (\alpha_{\parallel} + 2\alpha_{\perp})/3$ where α_{\parallel} and α_{\perp} are the polarizability parallel and perpendicular to the molecular axis, respectively].

The induced dipole force, $F = -\nabla U$, exerted on a molecule is proportional to the gradient of the intensity. Using $I(x, y, z, t) = I_0 \exp[-2(x^2 + y^2)/\omega_0^2] \exp(-4 \ln 2 t^2/\tau^2)$ (we probe near $z = 0$), the y component of the dipole force, F_y , is given by

$$F_y = -4 \frac{U_0}{\omega_0^2} y \exp\{-2[(v_{\parallel} t)^2 + y^2]/\omega_0^2\} \times \exp\left\{-4 \ln 2 \left(\frac{t^2}{\tau^2}\right)\right\}, \quad (3)$$

where U_0 is the Stark shift at the peak of the laser pulse in both space and time and $x = -v_{\parallel} t$ describes the motion of the molecules along the molecular beam direction. For $\Delta v_y \tau \ll y$, the experimentally observed velocity shift is given by $\Delta v_y = (1/m) \int_{-\infty}^{\infty} F_y(t) dt$ yielding

$$\Delta v_y = -\frac{4\sqrt{\pi}U_0}{\sqrt{2}m\omega_0 v_{\parallel}} \frac{1}{\sqrt{1 + 2 \ln 2[(\omega_0/v_{\parallel})/\tau]^2}} y \times \exp(-2y^2/\omega_0^2). \quad (4)$$

Equation (4) shows that the data points in Fig. 4 should have a dispersionlike shape. In both Figs. 4(a) and 4(b), the solid line corresponds to the normalized derivative of the spatial intensity profile of the YAG beam. In Fig. 4(b) deviation of the data points from the dispersion curve are observed for molecules deflected away from the microchannel plate detector. This deviation disappears when the deflecting laser intensity is lowered and ionization caused by the YAG beam is absent. We ascribe the deviation to the influence of the charge produced by the deflecting YAG beam. Molecular ions produced by the YAG, although produced 25 ns earlier than those ions produced by the CPM beam, have only moved about a micron during that 25 ns. They have therefore not left the focal volume before the femtosecond pulse probes the deflected molecules. Molecular ions from molecules that are deflected away from the microchannel plate detector (positive direction) interact with these YAG produced molecular ions much more strongly than molecules deflected toward from the detector.

Equation (4) can be used to estimate the depth of the Stark potential, U_0 based on the experimental measurements and to compare with the results obtained from Eq. (2) for I_2 and CS_2 (see next section). Solving Eq. (4) for U_0 at $y = \omega_0/2$ (where the acquired transverse velocity is maximum) yields $U_0 = 7$ meV for CS_2 and $U_0 = 6.6$ meV for I_2 .

V. ACHIEVABLE MAGNITUDES OF THE LASER-INDUCED DIPOLE POTENTIAL

The polarizabilities of atoms and small molecules are well known. Assuming that the static values [18] can be used at $1.06 \mu\text{m}$ we expect from Eq. (2) $U_0 = 10$ meV at $I = 9 \times 10^{11} \text{ W/cm}^2$ for CS_2 and $U_0 = 12$ meV for I_2 . There are a number of uncertainties in our experiment. For example, only $1\text{-}\mu\text{m}$ error in measuring ω_0 of the deflection beam leads to 25% error in the intensity. In addition, we expect the experiment to underestimate U_0 since the spatial resolution of the measurement is still limited. The measured and calculated values of U_0 agree within our experimental accuracy.

Our theoretical estimate of the Stark potential ignores any molecular alignment to the laser field either for CS_2 or for I_2 . However, the alignment potential, given by $U_A = -\frac{1}{4}(\alpha_{\parallel} - \alpha_{\perp})E^2$ exceeds 10 meV for CS_2 in a $9 \times 10^{11} \text{ W/cm}^2$ laser field. With an expected rotational temperature of 5 K [19] we should expect an average angular spread of about 30° about the direction of polarization for linearly polarized light [20] and then α_{\parallel} must replace α in Eq. (2) (that is, $U \approx -\frac{1}{4}\alpha_{\parallel}E^2$) and $\alpha_{\parallel}(\alpha_{\parallel} = 17.3 \times 10^{-40} \text{ C m}^2/\text{V}$ for CS_2) is almost twice α ($\alpha = 9.6 \times 10^{-40} \text{ C m}^2/\text{V}$ for CS_2).

Experimentally, we find no difference between the deflection using linear and circular polarization in Fig. 4(b) indicating that alignment does not play a significant role in our experiment, even for rotationally cooled molecules. We believe that the reason that we do not see significant alignment is that the longitudinal mode beating of our non-transform-limited YAG laser pulse gives rise to unobserved temporal

structure on the pulse. This approximately 50-ps structure introduces a fluctuating potential that rotationally heats the molecules.

The potential well that we measure through the nonresonant laser-induced dipole force is approximately 4 orders of magnitude larger than the typical potential depths reached in continuous waves studies on atoms (on the order of $1 \mu\text{eV}$ [10,21]). Thus to trap molecules with the nonresonant dipole force will require much less cooling than is typical in atomic trapping experiments. The Stark potential is proportional to the laser intensity, so the maximum potential well depth that can be achieved is limited by the maximum achievable intensity without ionization [2,7,22,23]. For CS_2 (I_2), with its ionization potential of 10.1 eV (9.3 eV), the tunnel ionization rate equals 10^6 s^{-1} at an intensity of $8 \times 10^{12} \text{ W/cm}^2$ ($5 \times 10^{12} \text{ W/cm}^2$). Although multiphoton ionization does not exhibit threshold behavior, the ionization rate is a very non-linear function of the laser intensity and a rate of 10^6 s^{-1} can be taken as an approximate effective threshold. This rate is particularly appropriate for our 10-ns pulse duration since it corresponds to about only 1% ionization during a 10-ns pulse. For these intensities Eq. (2) predicts a potential well depth of about $\sim 90 \text{ meV}$ for CS_2 and $\sim 70 \text{ meV}$ for I_2 . The slightly lower ionization potential of iodine molecules is compensated by its higher polarizability and consequently the maximum Stark shift remains about the same. At this laser field strength many molecules should align with the field (the alignment potential would be approximately 100 meV for CS_2) making the total well depth even greater.

In our YAG results we could not achieve this average intensity without ionization for two reasons. First, our Nd:YAG laser produces multilongitudinal mode output, which gives rise to transient spikes of higher peak intensity than would occur for a pulse with a smooth temporal profile. Since multiphoton ionization is highly nonlinear, the high-intensity spikes limit the average intensity that can be employed before multiphoton ionization occurs. Second, for $1.06 \mu\text{m}$ light illuminating I_2 or CS_2 , we do not satisfy the conditions for tunnel ionization [23] although we have used the tunneling approximation to calculate the maximum field that we can use. Other multiphoton ionization processes [24] raise the ionization rate and therefore lowers the peak intensity at which significant ionization is reached. Using $10.6 \mu\text{m}$ light places us securely in the tunneling limit [7,23]. We now demonstrate that deflection is also observable with a $10\text{-}\mu\text{m}$ deflection field.

VI. EXPERIMENTAL RESULTS WITH $10.6\text{-}\mu\text{m}$ DEFLECTION BEAM

The pulsed 10-Hz CO_2 laser consisting of a hybrid TEA CO_2 oscillator and a double-passed TEA CO_2 amplifier produced a $10.6\text{-}\mu\text{m}$ pulse with approximately 50% of the pulse energy of 600 mJ in a 70-ns (FWHM) gain switched peak. The remaining part of the energy was contained in a long tail that is not used in this experiment. The temporal structure of the pulse was monitored to ensure single longitudinal mode operation using a photon-drag detector.

Because of the high energy of the CO_2 pulse it was not possible to use the same focusing procedure as described above for the YAG laser. Figure 5 shows the experimental

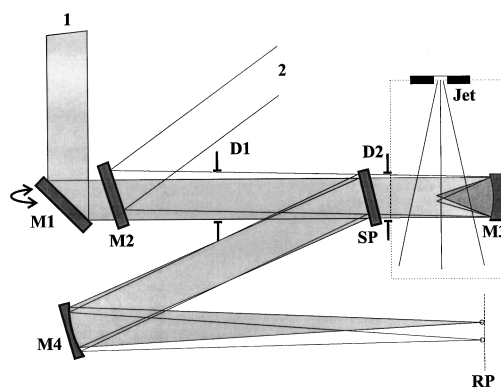


FIG. 5. Experimental schematic showing the optical arrangement used to position the CO_2 (deflection) beam (1) and the dye (measurement) beam (2). $M1$, $M3$, and $M4$ are gold-coated mirror. $M1$ is flat, $M2$ is a germanium plate used as a beam splitter, $M3$ is an $f/2$ parabolic mirror with focal length of 5 cm while the radius of curvature of $M4$ is $R=2 \text{ m}$. SP is a NaCl window used to reflect a small sample of the beam for alignment purposes. The focal properties of the beam inside of the chamber were imaged of the reference plane RP.

arrangement used with the CO_2 deflection beam. The CO_2 (deflection) and dye (measurement) beams were combined using a Ge window ($M2$ in Fig. 5) antireflection coated for $\lambda = 10.6 \mu\text{m}$ and reflective at $0.625 \mu\text{m}$. The beam diameters were approximately 2 and 1 cm at $\lambda = 10.6 \mu\text{m}$ and $\lambda = 0.6 \mu\text{m}$, respectively. Using two diaphragms ($D1$ and $D2$), the beams were aligned with an accuracy of about 2–4 mrad along the mirror axis of the 5-cm focal-length, 2.5-cm-diameter ($f/2$) parabolic mirror ($M3$ in Fig. 5), mounted inside the vacuum chamber.

We measured the diameter of the focal spot at $\lambda = 10.6 \mu\text{m}$ with the CO_2 amplifier switched off. For that measurement the parabolic mirror $M3$ was placed outside the vacuum chamber. A 5-mm-thick NaCl window was mounted in front of the mirror at the angle of 45° with respect to the incident beam. A $25\text{-}\mu\text{m}$ -diameter pinhole was scanned in the vicinity of the waist of the CO_2 beam reflected from the NaCl window. The measured focal spot diameter is about $35 \mu\text{m}$ (FWHM). Thus, we estimate the intensity in the beam waist as $4.5 \times 10^{11} \text{ W/cm}^2$.

We used a reference beam to properly adjust the relative position of the deflection and the probe foci. A wedged ($\sim 2 \text{ in.}$) NaCl window (SP in Fig. 5) reflected approximately 4% of the incident radiation at both wavelengths. Using a 1-m focal-length gold-coated mirror ($M4$ in Fig. 5) the foci of the reflected beams are projected onto the reference plane (RP in Fig. 5) producing a magnified ($\times 20$) image of the measurement area inside the vacuum chamber. We adjusted the relative position of the beam waists in the jet by tilting the infrared beam ($\sim 0.1^\circ$) in the vertical direction so that the CO_2 beam shifted $25 \mu\text{m}$ upstream of the CPM laser focus. In that case it takes the molecules about 75 ns to travel from the center of the deflection beam to the probed volume (note: argon was used as the buffer gas for these measurements).

Each time-of-flight spectrum was a result of averaging over 250–500 shots. There was no ionization by the CO_2 laser pulse. To eliminate the influence of the timing jitter

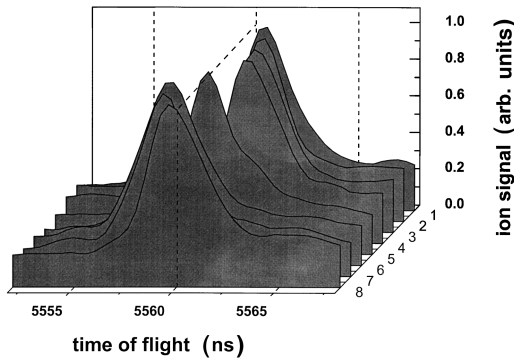


FIG. 6. Ion spectra for successive 12- μm steps between the relative positions of the deflecting and measurement beams.

between the CO_2 and dye pulses, time-of-flight spectra were only recorded if the two pulses arrived at the proper delay.

Figure 6 shows the successive CS_2^+ spectra recorded at different horizontal positions of the deflecting beam. Just as for CS_2 molecules deflected by the YAG beam one can see a definite shift in the temporal position of the ion spectra. In Fig. 7 we have plotted the temporal shift of the maximum of the time-of-flight spectra and the corresponding Δv_y versus horizontal position of the deflecting beam for three successive scans. The solid line corresponds to the normalized derivative of a Gaussian profile with $\omega_0 = 30 \mu\text{m}$. This magnitude is in agreement with our estimated beam waist of the infrared beam.

The data in Fig. 7 are more symmetric than those obtained using the YAG laser. We observed no ionization of the CS_2 molecules up to $5 \times 10^{11} \text{ W/cm}^2$, the highest intensity that we could achieve. Consequently, there are no space-charge effects. Moreover, the bigger diameter of the waist of the CO_2 beam allows higher relative resolution of measurement.

Assuming the Gaussian shape of the curve with $\omega_0 = 30 \mu\text{m}$ we obtain $U_0 = 4 \text{ meV}$ from Eq. (4). This value can be compared to a well depth of about 4.5 meV obtained using $U = -\frac{1}{4}\alpha E^2$ [Eq. (2)] at our estimated operating intensity of $4 \times 10^{11} \text{ W/cm}^2$.

VII. DISCUSSION AND CONCLUSIONS

A. Maximum Stark shifts

We have studied two molecules that have relatively large polarizabilities ($\alpha = 9.6 \times 10^{-40} \text{ C m}^2/\text{V}$ for CS_2 and $\alpha \approx 12.1 \times 10^{-40} \text{ C m}^2/\text{V}$ for I_2) and we have noted that the maximum Stark shift that can be achieved for I_2 and CS_2 should be approximately the same. In general, any neutral atom or small molecule has approximately the same maximum Stark shift although the polarizability can vary greatly. This is because, as the molecular polarizability decreases, the ionization potential increases and the increase in the maximum intensity that the molecule can withstand [2,22] roughly compensates for the decreasing polarizability. For example, we predict that H_2 , a very unpolarizable molecule, can experience a 50-meV Stark shift at an intensity [2,22] where the tunnel ionization rate reaches our reference value of 10^6 s^{-1} . Even helium, a very unpolarizable atom and Cs, a very polarizable atom can support a maximum Stark

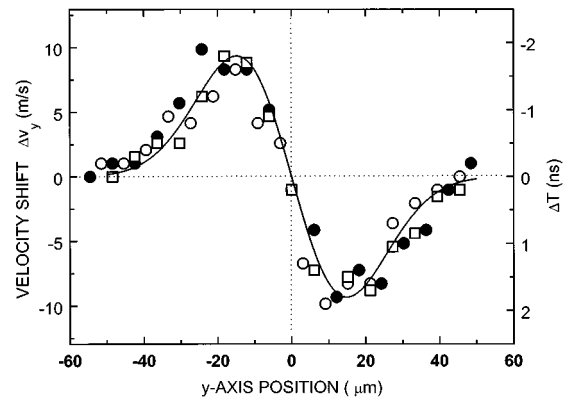


FIG. 7. The dependence of CS_2^+ time of flight (left axis) and transverse velocity (right axis) on the relative displacement of the deflecting and measurement beams. Open and filled circles and squares correspond to three successive scans with realignment. Solid curve is a derivative of the Gaussian curve with FWHM 35 μm .

shift of approximately 30 meV at the intensity where their ionization rates approach 10^6 (for He this intensity is $2.6 \times 10^{14} \text{ W/cm}^2$ and for Cs, $3.5 \times 10^{11} \text{ W/cm}^2$). Therefore, the deflection that we have demonstrated above, and the consequences discussed below, are very general.

B. Focusing of molecules

In addition to showing control over the external variables of a molecule through the nonresonant laser-induced dipole force, we have also shown a method of focusing molecules. The data in both Fig. 4 and in Fig. 7 show that molecules that pass near the center of the deflection beam gain a velocity that is proportional to their distance from the center. These molecules must meet at a common point below the laser focus. For example, in the CO_2 data in Fig. 7, the molecules gain a transverse velocity of 5 m/s at an offset from the beam center of 5 μm . These molecules will reach the axis (defined by the line joining the aperture and the center of the laser beam) in 1 μs . During that time the CS_2 molecules, moving with a longitudinal velocity of 500 m/s, travel 500 μm . Consequently the focal length of the molecular lens is $f \approx 500 \mu\text{m}$.

This experiment demonstrates one-dimensional focusing. Two deflection laser beams at right angles to each other would produce two-dimensional focusing as would a laser beam focused through an axicon.

C. Two-dimensional trapping: Molecular quantum wires

A dramatic implication of the results that we have just described is the possibility of forming molecular (or atomic) quantum wires. That is, confining molecules (or atoms) in two dimensions with confinement so strong that their transverse translational energy is quantized. Molecules propagating in a molecular quantum wire would be the analog of light propagating in an optical fiber. What makes molecular quantum wires especially exciting is that it appears that molecules can be confined to within about 10–60 \AA , not much larger than a molecular dimension.

Producing a molecular quantum wire does not require a large extrapolation over the present experiment. Consider the output of a long-pulse 1.06- μm laser focused to produce a line of high-intensity radiation. Such a line can be achieved using an axicon or a hollow core waveguide. Alternatively, a standing wave pattern produced by counterpropagating beams in two perpendicular directions produces an array of molecular quantum wires. The diameter of a line focus can be less than one wavelength of light (the FWHM diameter of a standing wave is approximately $\lambda/4$) providing a confinement potential in two dimensions that is required for the molecular quantum wire. The length of the line focus is not confined by physics, but is, of course, confined by the size and complexity of the laser required.

It is possible to calculate the zero-point energy of such a trap. Assuming the confinement potential characteristic of a standing wave in one dimension $U_0 \cos^2(2\pi r/\lambda)$, the potential well structure near the well minimum is given by $U = -U_0[1 - (2\pi^2/\lambda^2)r^2]$ so the zero-point energy of the ground state is $E_g = \pi\hbar U_0^{1/2}/\lambda m^{1/2}$. For realistic parameters, $\lambda = 1 \mu\text{m}$, $U_0 = 50 \text{ meV}$ and taking the H_2 mass for m , we obtain $E_g = 10^{-4} \text{ eV}$. The approximate dimensions of the ground-state wave function would be about 60 Å. For larger mass molecules the zero-point energy is reduced as is the diameter of the ground-state wave function. Having determined the level spacing in the quantum wire we now discuss the issues involved in coupling molecules into the fundamental mode of the wire.

In our molecular deflection experiment, the molecular beam had an estimated lateral kinetic energy E_{kin} of about 10^{-7} eV in the region of the laser focus. This is orders of magnitude less than the zero-point energy in the molecular wire. Since the lateral kinetic energy of the beam is given by $E_{\text{kin}} = \frac{1}{2}mv_{\perp}^2 = \frac{1}{2}mv_x^2 \sin^2\vartheta$ where $\vartheta = d/2l$, it is clear that the lateral kinetic energy can even be reduced if v_x or m is reduced.

The major problem to be overcome before molecular quantum wires are produced is coupling this beam of molecules into the wire without simultaneously coupling too much of their longitudinal energy into transverse motion. In analogy with optical fibers where laser light is coupled into the fundamental mode of the fiber using lenses, we believe that molecular lenses, such as we have just described, will be very helpful.

D. Three-dimensional trapping: Molecular quantum dots

The approximately $\lambda/4$ dimensions of a two-dimensional trap can also be achieved in three dimensions. With well depths of 50–100 meV the zero-point energy will again be approximately 10^{-4} eV . It is clear that trapping is possible even for molecules at or near room temperature. For a molecular temperature of approximately 1 degree K the ground state will be preferentially populated. Methods for cooling have been discussed [4,21]. However, molecules in such a trap will interact differently than in free space. Laser-induced van der Waals complexes will play a major role and must be considered [25].

E. An accelerator for neutral molecules

If the Stark shift can be on the order of 100 meV, approximately one order of magnitude greater than those measured

here, the gradient of the Stark shift can be much larger still. The largest intensity gradient that can be produced without a surface present occurs in standing waves where the region of highest and lowest intensity are separated by 0.25λ . This is almost two orders of magnitude smaller than the scale length of the intensity gradient that we have used and should lead to much higher acceleration.

Molecules trapped in a standing wave can be accelerated if the pattern is accelerated. Acceleration of a standing wave pattern is possible using an appropriately chirped pulse. The velocity V_a of a pattern is determined by the frequency difference $\delta\nu$ between the counterpropagating beams $\delta\nu = 2V_a/\lambda$. Since the maximum force is constant, the velocity will increase linearly with time so the frequency chirp that is required to follow the molecules' motion is linear. The technology of pulse shaping and chirping is well advanced [26] and linearly chirped pulses covering a wide frequency range are readily produced.

In an optimally accelerated standing wave with a gradient of the Stark shift of $4 \times 10^5 \text{ V/m}$, a hydrogen molecule will achieve a velocity $V_a = 20 \text{ km/s}$ in 1 ns corresponding to a kinetic energy of 4 eV. For such a short acceleration length, the maximum frequency difference $\delta\nu$ between the counterpropagating beams is only about 40 GHz. Since the kinetic energy increases quadratically with time a kinetic energy of 400 eV is possible after 10 ns and the required frequency chirp is within the bandwidth of a picosecond pulse. The requirements necessary for this acceleration are available in many laboratories today. Accelerating neutral rotationally and vibrationally cold molecules to hundreds of keV energies appears feasible.

F. Excited states

Although this paper has only explicitly discussed ground-state molecules or atoms, the polarizability can be much larger for excited states than for the ground state [27]. Thus, for a given laser intensity the ground and excited states of a molecule experience different Stark shifts and therefore can be spatially separated according to their electronic state. In addition, since Stark shifts are dependent on the internuclear coordinates, intense nonresonant radiation modifies the potential energy surfaces of a molecules and consequently the internal dynamics. In general, the nonresonant laser-induced Stark shifts provide us with robust methods for manipulating the external and internal variables of quantum systems.

ACKNOWLEDGMENTS

The authors acknowledge financial support from NATO laboratory linkage Grant No. LG 921398, enabling this international collaboration to occur. In addition, E.C. thanks the International Council of Canadian Studies and C. Ellert thanks the A. V. Humboldt Foundation for financial support. The experiment benefited from the technical assistance of David Joines, Daniel Roth, and Bert Avery. We appreciate discussions with NRC colleague Tamar Seideman, who, parallel with these experiments, has modeled molecular focusing. Helpful discussions with Misha Ivanov and Albert Stolow are also gratefully acknowledged.

- [1] P. B. Corkum, M. Yu Ivanov, and J. Wright, in *Annual Reviews of Physical Chemistry*, edited by H. Strauss, G. Babcock, and S. Leone (Annual Reviews Inc., Palo Alto, CA, 1997).
- [2] P. Dietrich and P. B. Corkum, *J. Chem. Phys.* **97**, 3187 (1992); *Comments At. Mol. Phys.* **28**, 357 (1993); F. Ilkov *et al.*, *Phys. Rev. A* **51**, R2695 (1995).
- [3] P. Dietrich *et al.*, *Phys. Rev. A* **47**, 2305 (1993).
- [4] B. Freidrich and D. Herschbach, *Phys. Rev. Lett.* **74**, 4623 (1995).
- [5] T. Seideman, *J. Chem. Phys.* **106**, 2881 (1997).
- [6] H. Stapelfeldt, H. Sakai, E. Constant, and P. B. Corkum, *Phys. Rev. Lett.* **79**, 2787 (1997).
- [7] P. B. Corkum, N. H. Burnett, and F. Brunel, *Phys. Rev. Lett.* **62**, 1259 (1989).
- [8] T. B. Simpson *et al.*, *J. Chem. Phys.* **83**, 628 (1985).
- [9] P. H. Bucksbaum, D. Schumacher, and M. Bashkansky, *Phys. Rev. Lett.* **61**, 1182 (1988); J. Chaloupka *et al.* (unpublished).
- [10] See, for example, papers in *Atomic Physics 14*, AIP Conf. Proc. No. 323, edited by D. J. Wineland, C. E. Weiman, and S. J. Smith (American Institute of Physics, New York, 1994).
- [11] A. Ashkin, J. M. Dziedzic, and J. E. Bjorkholm, S. Chu, *Opt. Lett.* **11**, 288 (1986).
- [12] S. K. Svoboda and S. Block, *Annu. Rev. Biophys. Biomol. Struct.* **23**, 247 (1994); A. Ashkin and J. M. Dziedzic, *Science* **235**, 1517 (1987); T. T. Perkins *et al.*, *Science* **264**, 822 (1994).
- [13] H. Stapelfeldt, E. Constant, and P. B. Corkum, *Phys. Rev. Lett.* **74**, 3789 (1995).
- [14] D. R. Miller, in *Atomic and Molecular Beam Methods*, edited by B. Scoles (Oxford University Press, New York, 1988), p. 15.
- [15] C. Rolland and P. B. Corkum, *Opt. Commun.* **59**, 64 (1986).
- [16] P. B. Corkum, N. H. Burnett, and F. Brunel, in *Atoms in Intense Fields*, edited by M. Gavrilu (Academic Press, New York, 1992), p. 109.
- [17] A. A. Radzig and B. M. Smirnov, *Reference Data on Atoms, Molecules and Ions* (Springer-Verlag, New York, 1085).
- [18] K. J. Miller, *J. Am. Chem. Soc.* **112**, 8543 (1990).
- [19] D. T. Cramb, H. Bitto, and J. R. Huber, *J. Chem. Phys.* **96**, 8761 (1992).
- [20] M. Yu. Ivanov (unpublished).
- [21] J. T. Bahns, W. C. Stwalley, and P. L. Gould, *J. Chem. Phys.* **104**, 9689 (1996).
- [22] M. V. Ammosov, N. B. Delone, and V. P. Krainov, *Zh. Eksp. Teor. Fiz.* **91**, 2008 (1986) [*Sov. Phys. JETP* **64**, 1191 (1986)].
- [23] L. V. Keldysh, *Zh. Eksp. Teor. Fiz.* **47**, 1945 (1964) [*Sov. Phys. JETP* **20**, 1307 (1965)].
- [24] B. Walker *et al.*, *Phys. Rev. Lett.* **73**, 1227 (1994).
- [25] M. Yu Ivanov, D. R. Matusek, and J. S. Wright, *Phys. Rev. A* **54**, 5159 (1996).
- [26] A. M. Weiner, J. P. Heritage, and R. N. Thurston, *Opt. Lett.* **11**, 153 (1986).
- [27] R. W. Molof *et al.*, *Phys. Rev. A* **10**, 1131 (1974).